J. Eng. Technol. Sci., Vol. 54, No. 5, 2022, 220507

An Improved Capillary Pressure Model for Fractal Porous Media: Application to Low-Permeability Sandstone

Muhammad Saafan*, Mysara Mohyaldinn & Khaled Elraies

Department of Petroleum Engineering, Universiti Teknologi PETRONAS (UTP), 32610 Seri Iskandar, Perak Darul Ridzuan, Malaysia
*E-mail: muhammad.saafan@yahoo.com

Highlights:

- A new representation of the pore structure was proposed.
- An analytical fractal capillary pressure model was derived.
- Model validation using experimental data was conducted.

Abstract. Capillary pressure is a crucial input in reservoir simulation models. Generally, capillary pressure measurements are expensive and time-consuming; therefore, there is a limitation on the number of cores tested in the laboratory. Accordingly, numerous capillary pressure models have been suggested to match capillary pressure curves and overcome this limitation. This study developed a new fractal capillary pressure model by depicting the porous system as a bundle of tortuous triangular tubes. The model imitates the pores' angularity, providing a more accurate representation of the pore system than smooth circular openings. Moreover, triangular tubes allow the wetting phase to be retained in the tube's corners. A genetic algorithm was employed to match the capillary pressure curves and obtain the proposed model's parameters. Capillary pressure data of eight low-permeability sandstone samples from the Khatatba formation in the Western Desert of Egypt were utilized to test the proposed model. The results revealed that the developed model reasonably matched the laboratory-measured data.

Keywords: *capillary pressure curves; fractal model; fractal porous media; genetic algorithm; pore structure modeling.*

1 Introduction

Capillary pressure is a rock-fluid property critical for several recovery processes [1]. Capillary pressure governs the reservoir's fluid distribution and determines the amount of hydrocarbon remaining after primary recovery. Moreover, capillary pressure is important in CO_2 flooding as it controls trapping mechanisms such as the residual trapping [2,3]. The capillary pressure should be correctly represented in reservoir simulations to assess the reserves accurately. For instance, a 5% inaccuracy in capillary pressure data results in a difference of millions of barrels in estimated reserves. Capillary pressure is commonly quantified as a function of saturation in the laboratory; however, laboratory

Received 28 April 2022, Revised 9 June 2022, Accepted for publication 17 June 2022
 ISSN: 2337-5779,
DOI: 10.5614/j.eng.technol.sci.2022.54.5.7

.

measurements are costly and time-consuming. Therefore, capillary pressure models are necessary to overcome these limitations [4]. Recently, multiple attempts have been made to estimate capillary pressure curves by constructing pore network models using rock images [5,6].

Numerous studies have demonstrated the fractal properties of porous media [7,8]. Fractal theory has found several applications in reservoir engineering, including modeling of permeability [9,10], capillary pressure [11-13], and electrical conductivity [14,15]. Li in [16] developed a capillary pressure model for heterogeneous and fractured rocks that reduced to Brooks and Corey's model at specified fractal dimension values, D_f. Cai, *et al*. in [17] investigated spontaneous imbibition in gas saturated rock using fractal theory and the capillary tube model. Gao, *et al.* in [18] suggested a fractal representation for the J-function that incorporates the Leverett J-function and fractal theory. Saafan & Ganat in [11] derived a capillary pressure model from modeling the porous system as straight equilateral triangle tubes.

The previous fractal models simplified the pore structure by depicting it as a bundle of cylinders. However, the actual pore geometries exhibit angularity, allowing the wetting phase to persist in pore corners. As a result, representing pores as triangle tubes is more appropriate. The primary goal of this study is to propose a novel fractal capillary pressure model using a unique representation of a porous medium to overcome the shortcomings of the existing simplifications. This study simulated the pore morphology as tortuous triangular tubes, and their numbers follow a fractal scaling law. The capillary entry pressure was expressed in terms of the inscribed radius of the triangular pores utilizing the MSP approach. Additionally, an analytical capillary pressure model was developed using the newly proposed system representation. A genetic algorithm was used for matching laboratory measure capillary pressure data and obtaining the fractal model parameters. Eight low-permeability samples from the Khatatba formation in the Western Desert of Egypt were utilized for validating the proposed model. The results indicated that the constructed model reasonably matched the capillary pressure data of the low-permeability samples.

2 Methods

2.1 Pore System Representation

Porous media exhibit a sophisticated pore structure, in which the pores have a broad irregular shape. The pore shape factor, G, is utilized to represent the pore morphology and is determined from [19]:

$$G = \frac{A}{P^2} \tag{1}$$

where A denotes the pore's area, and P denotes its perimeter.

A circular pore has a shape factor of 1/4π, while a square pore has a shape factor of 1/16. For triangular pores, G is less than or equal to $\sqrt{3}/36$. Wu, *et al.* determined a sample's pore shape factor using micro-CT analysis, as illustrated in Figure 1 [20]. The shape factor distribution in Figure 1 demonstrates that modeling the pore structure with circular tubes did not accurately depict the pore structure of this core sample. On the other hand, most pores have pore shape factors that can be represented as tubes with equilateral triangular cross-sections and $G = \sqrt{3}/36$. The pore system is represented in this work as tortuous equilateral triangular tubes, as shown in Figure 2.

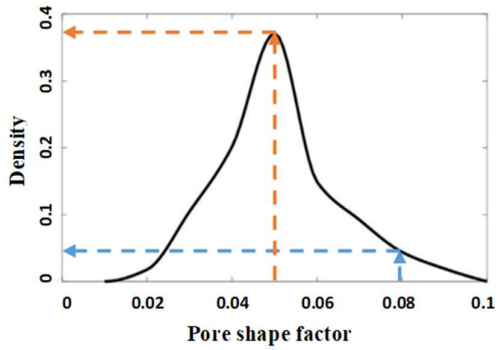

Figure 1 Pore shape factor from the micro-CT analysis [20].

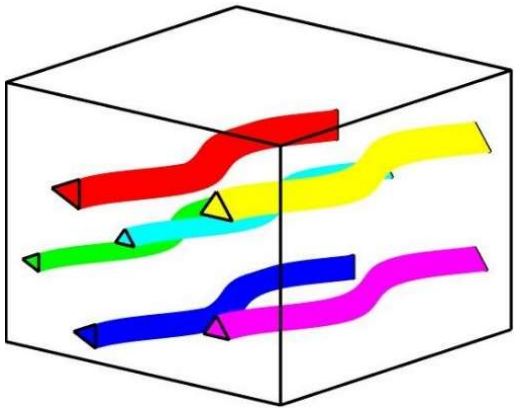

Figure 2 Pore structure representation.

.

2.2 Entry Capillary Pressure in Triangular Tubes

The Mayer-Stowe-Princen (MSP) method is used to determine the capillary entry pressure of a particular tube for a water-oil system as [21]:

$$\sum_{i=o,w} P_i dV_i = \sum_{ij=ow,os,ws} \sigma_{ij} dA_{ij} \quad (2)$$

where dV_i is the change in volume of phase i, σ_{ij} and dA_{ij} are the interfacial tension and the change of interfacial area between phases i and j. Eq. (2) is expanded in the following form:

$$P_o dV_o + P_w dV_w = \sigma_{ow} dA_{ow} + \sigma_{os} dA_{os} + \sigma_{ws} dA_{ws} \quad (3)$$

For a rigid solid phase, the following equations are satisfied:

$$dV_s = dV_o + dV_w = 0 \quad (4)$$

$$dA_s = dA_{os} + dA_{ws} = 0 \quad (5)$$

Using Young's equation, the interfacial tension between the distinct phases is related to the contact angle as:

$$\sigma_{os} - \sigma_{ws} = \sigma_{ow} \cos\theta_r \quad (6)$$

where θ_r is the receding contact angle. From Eqs. (3)-(6), the threshold capillary pressure is expressed as:

$$P_c = P_o - P_w = \frac{\sigma_{ow}(dA_{ow} + \cos\theta_r \, dA_{os})}{dV_o} \quad (7)$$

Figure 3 shows the remaining water at the corners of an invaded triangle tube. The threshold capillary entry pressure is calculated from:

$$P_c = \frac{\sigma_{ow} \cos\theta_r}{R}\left(1 + 2\sqrt{\pi G}\right) F_d \quad (8)$$

where F_d is expressed as:

$$F_d = \frac{1 + \sqrt{1 - \frac{4GC}{\cos^2\theta_r}}}{1 + 2\sqrt{\pi G}} \quad (9)$$

For a circular capillary, $F_d = 1$ and $G = 1/(4\pi)$, hence Eq. (8) is reduced to $P_c = 2\sigma \cos(\theta_r)/R$. For a triangular tube, C is given by:

$$C = \sum_{i=1}^{n} \left[\cos\theta_r \frac{\cos(\theta_r + \beta_i)}{\sin\beta_i} - \left(\frac{\pi}{2} - \theta_r - \beta_i\right)\right] \quad (10)$$

where β denotes corner half-angles, and n denotes the number of corners, satisfying:

$$\beta_i < \frac{\pi}{2} - \theta_r \quad (11)$$

The remaining water in the tube corners (Figure 3) is computed as [22]:

$$A_{wr} = C\left(\frac{\sigma_{ow}}{P_c}\right)^2 \tag{12}$$

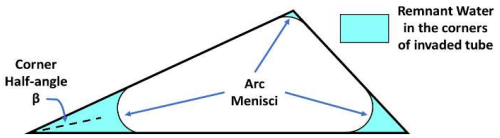

Figure 3 Remaining water in the corners of an invaded triangle tube [11].

2.3 New Capillary Pressure Model

The number of triangle tubes with radii larger than or equal to R required for filling a fractal porous media is [9]:

$$N = \left(\frac{R_{max}}{R}\right)^{D_f} \tag{13}$$

where R_{max} is the greatest capillary's inscribed radius. The number of capillary tubes, dN, between two radii is found by differentiating Eq. (13) as:

$$dN = -D_f\, R_{max}^{D_f}\, R^{-D_f-1}\, dR \tag{14}$$

The tortuous length of a capillary is represented as [9]:

$$L_t = 2^{1-D_t} R^{1-D_t} L_0^{D_t} \tag{15}$$

where L_0 denotes the straight capillary length, and D_t denotes the tortuosity fractal dimension, typically between 1 and 2. The total volume of the pores (Figure 2) is computed as:

$$V_p = \int_{R_{min}}^{R_{max}} AL_t\,(-dN) \tag{16}$$

where A is the cross-sectional area of a tube and is expressed as [19]:

$$A = \frac{R^2}{4G} \tag{17}$$

Using Eqs. (14), (15), and (17), the integration of Eq. (16) is represented as:

$$V_p = \alpha\, R_{max}^{D_f}\left(R_{max}^{3-D_f-D_t} - R_{min}^{3-D_f-D_t}\right) L_0^{D_t} \tag{18}$$

where α is expressed as:

$$\alpha = \frac{D_f}{2^{D_t+1}\, G\,(3-D_f-D_t)} \tag{19}$$

The remaining water volume in the entire system is computed from:

.

$$V_w = \int_{R_{min}}^{R} AL_t(-dN) + \int_{\mathrm{R}}^{R_{max}} A_{wr}L_t(-dN) \tag{20}$$

where R is the smallest tube's radius that will be invaded at a given P_c, as in Eq. (8). The first integration in Eq. (20) denotes the water remaining in uninvaded tubes and is calculated as:

$$\int_{R_{min}}^{R} AL_t\,(-dN) = \alpha\, R_{max}^{D_f} \left(R^{3-D_f-D_t} - R_{min}^{3-D_f-D_t}\right) L_0^{D_t} \tag{21}$$

The second integration in Eq. (20) is the residual water in the invaded tubes' corners, as illustrated in Figure 3, and is computed as:

$$\int_{\mathrm{R}}^{R_{max}} A_{wr}L_t\,(-dN) = \frac{2^{1-D_t} C\, r^{2D_f} R_{max}^{D_f} \left(R^{1-D_f-D_t} - R_{max}^{1-D_f-D_t}\right) L_0^{D_t}}{D_f+D_t-1} \tag{22}$$

Finally, the water saturation (S_w) at a particular capillary pressure is determined by dividing Eq. (20) by Eq. (18).

$$S_w = \frac{R^{3-D_f-D_t} - R_{min}^{3-D_f-D_t} + \dfrac{2^{1-D_t} C\, r^{2D_f} R_{max}^{D_f} \left(R^{1-D_f-D_t} - R_{max}^{1-D_f-D_t}\right)}{\alpha\left(D_f+D_t-1\right)}}{R_{max}^{3-D_f-D_t} - R_{min}^{3-D_f-D_t}} \tag{23}$$

Using Eq. (8), Eq. (23) is expressed in terms of P_c as:

$$S_w = \begin{cases} 1 & if\ P_c < P_e \\ \dfrac{\varepsilon\, P_c^{-2}\left(P_{c,max}^{D_f+D_t-1} - P_e^{D_f+D_t-1}\right)}{P_e^{D_f+D_t-3} - P_{c,max}^{D_f+D_t-3}} & if\ P_c > P_{c,max} \\ \dfrac{P_c^{D_f+D_t-3}\left\{1+\varepsilon\left[1-\left(\frac{P_e}{P_c}\right)^{D_f+D_t-1}\right]\right\} - P_{c,max}^{D_f+D_t-3}}{P_e^{D_f+D_t-3} - P_{c,max}^{D_f+D_t-3}} & otherwise \end{cases} \tag{24}$$

where P_e and $P_{c,max}$ are the entry pressures of the largest and smallest tubes, respectively. Also, ε is expressed as:

$$\varepsilon = \frac{2^{1-D_t}\, G\, C\, (3-D_f-D_t)}{cos^2\theta_r\, (1+2\sqrt{\pi G})^2\, F_d^2\, (D_f+D_t-1)} \tag{25}$$

2.4 Genetic Algorithm (GA)

Genetic algorithms apply Darwin's theory of evolution in optimization problems [23] and employs iterative approaches to move through generations of chromosomes (Figure 4) [24].

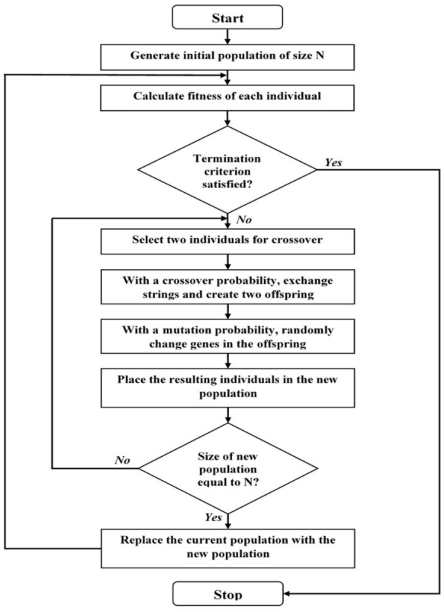

Figure 4 Process flow diagram of the genetic algorithm.

Natural selection ensures that only the fittest individuals survive and reproduce, passing their genes to the following generation. The most frequently utilized selection strategy in GA is roulette wheel selection. GA uses crossover to exchange information between parents to generate new offspring. The crossover procedure begins by randomly selecting a crossover point between the two parents. The parents' chromosomes are split and exchanged to make two offspring. Moreover, the mutation operator works by changing the values of genes from ones to zeros and vice versa, thereby improving the GA's performance and mitigating the problem of getting trapped in a local optima.

The GA was used to match the capillary pressure for the newly developed fractal model given by Eq. (24). Table 1 illustrates the search space of the model parameters used by the GA.

Table 1 GA search space of the different model parameters.

Parameter	Minimum value	Maximum value
D_f	1	2
D_t	1	2
P_e *(psi)*	0.01	50
$P_{c,max}$ *(psi)*	10^3	10^6

.

3 Results and Discussion

The capillary pressure measurements of eight low-permeability core samples from the Khatatba formation in Egypt's Western Desert were utilized to validate the developed model. Figure 5 shows the laboratory-measured capillary pressure.

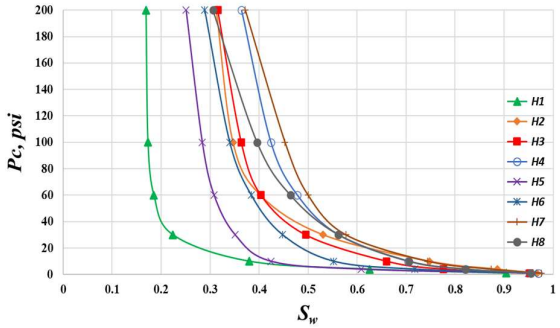

Figure 5 Capillary pressure data of the eight-core samples.

The GA was utilized to match the capillary pressure curves, and the matched parameters for the eight-core samples are shown in Table 2.

Table 2 Search space of the different parameters.

Sample	D_f	D_t	P_e (psi)	$P_{c,max}$ (kpsi)
H1	*1.291*	*1.340*	*0.761*	*99.37*
H2	*1.520*	*1.258*	*2.431*	*99.87*
H3	*1.572*	*1.251*	*1.177*	*85.96*
H4	*1.502*	*1.366*	*1.295*	*69.95*
H5	*1.683*	*1.105*	*0.473*	*98.74*
H6	*1.475*	*1.344*	*0.804*	*99.66*
H7	*1.565*	*1.301*	*1.935*	*39.68*
H8	*1.283*	*1.642*	*1.526*	*3.89*

The average absolute relative error (AARE) for the calculated water saturation is presented in Table 3. From error analysis, the capillary pressure curves of samples H1, H2, H3, H4, H5, H6, H7, and matched the experimental data with AARE of 9.89, 4.09, 2.33, 1.08, 7.02, 1.54, 1.07, and 1.77%, respectively.

Table 3 Error analysis in the calculated water saturation.

Sample	*ARE*	Sample	*ARE*
H1	*9.89*	*H5*	*7.02*
H2	*4.09*	*H6*	*1.54*
H3	*2.33*	*H7*	*1.07*
H4	*1.08*	*H8*	*1.77*

Finally, the developed model results versus the laboratory measurements are shown in Figure 6.

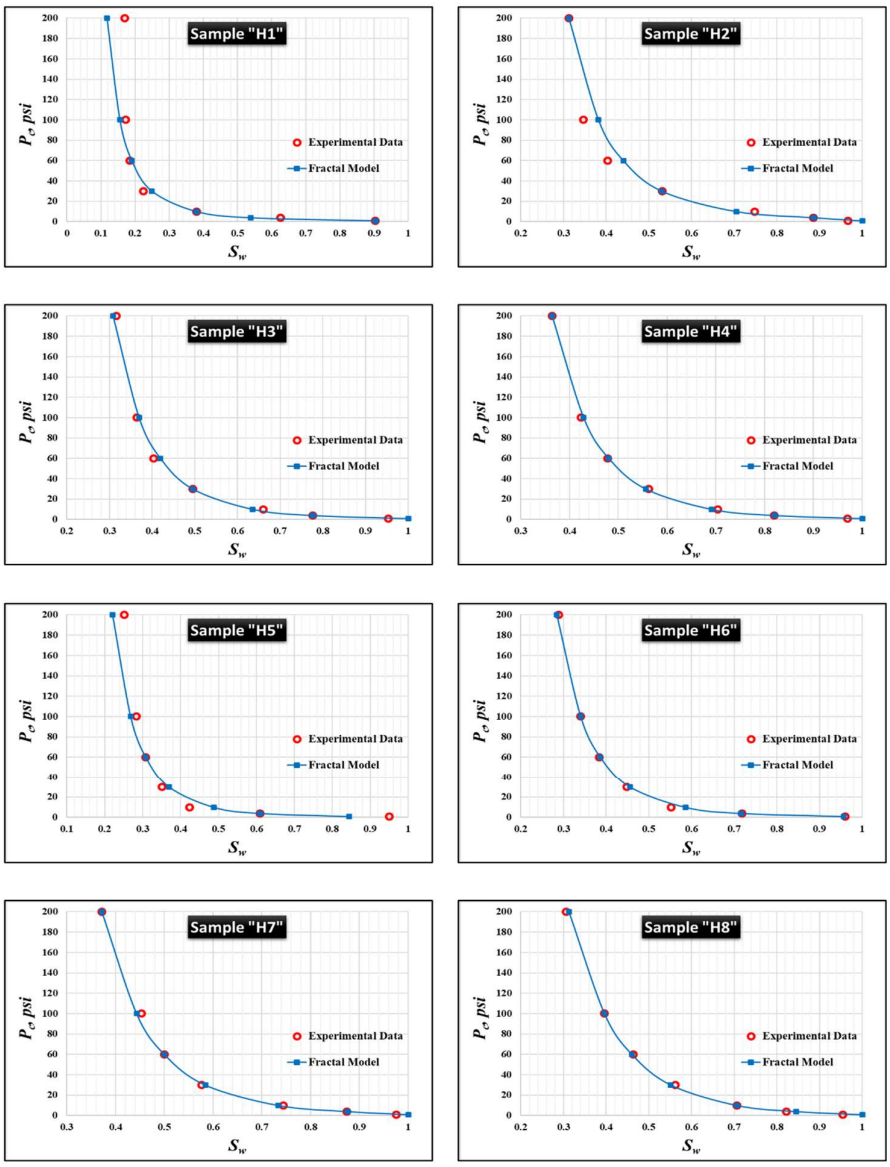

Figure 6 Matched capillary pressure curves of the eight-core samples.

.

Moreover, as shown in Figure 7, the error factor lines for matched versus measured water saturation of the eight samples were ±0.08. As a result of the above investigation, the created fractal model consistently matches the capillary pressure curves.

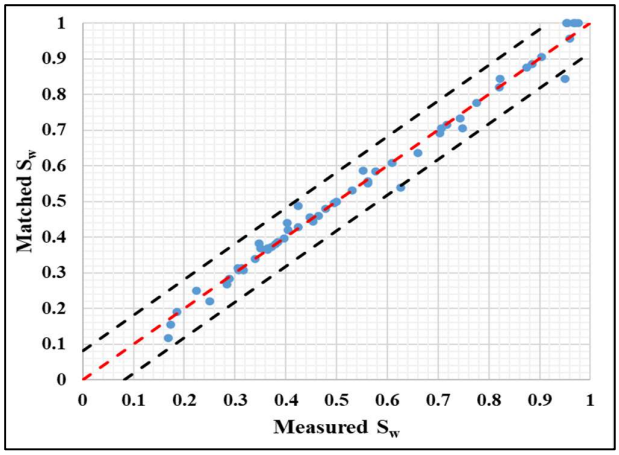

Figure 7 The matched versus measured S_w of the eight samples.

4 Conclusions

The capillary pressure is commonly measured in the laboratory, which is costly, challenging, and accompanied by measurement uncertainties, particularly for low-permeability samples. Hence, the number of cores examined in the laboratory is restricted. Capillary pressure models are thus required to overcome these restrictions.

This paper introduced a pore structure representation that uniquely described the porous media as a bundle of tortuous triangular tubes. Representing the pore system as a bundle of circular tubes does not depict the pore structure of actual rock, and no wetting phase is retained in the pores. The new representation is more appropriate to the actual pore structure and accounts for the residual water saturation in the corners of the pores. Moreover, a capillary pressure model was developed based on fractal theory. The GA was employed to match experimental capillary pressure data and obtain the fractal parameters. Based on the findings, the proposed model reasonably matched the capillary pressure curves of eight low-permeability samples.

References

[1] Kewen L., *Theoretical Development of the Brooks-Corey Capillary Pressure Model from Fractal Modeling of Porous Media*, Proc. SPE/DOE Symp. Improv. Oil Recover., **2004** April, Society of Petroleum Engineers, 2004. DOI:10.2523/89429-MS.

[2] Foroozesh, J., Dier M.A. & Rezk, M.G., *A Simulation Study on CO2 Sequestration in Saline Aquifers: Trapping Mechanisms and Risk of CO2 Leakage*. MATE, Web Conf., **225**, pp. 0-5, 2018. DOI:10.1051/matecconf/201822503004.

[3] Rezk, M.G., Foroozesh, J., Abdulrahman, A. & Gholinezhad, J., *CO2 Diffusion and Dispersion in Porous Media: Review of Advances*, Experimental Measurements and Mathematical Models, Energy & Fuels., **36**, pp. 133-55, 2022. DOI: 10.1021/acs.energyfuels.1c03552.

[4] Yang, J., Liu, Z., Chen, L. & Huang, Y., *New Mathematical Model for Predicting Capillary Pressure*, Chem Technol Fuels Oils, **53**, pp. 392-398, 2017. DOI:10.1007/s10553-017-0816-4.

[5] Foroozesh, J., Mohamed Abdalla, A.I., Zivar, D. & Douraghinejad, J., *Stress-Dependent Fluid Dynamics of Shale Gas Reservoirs: A Pore Network Modeling Approach*, J. Nat. Gas. Sci. Eng., **95**, 104243, 2021. DOI: 10.1016/j.jngse.2021.104243.

[6] Shabani, A., Zivar, D., Jahangiri, H.R. & Shahrabadi, A., *Application of Pore Network Modeling in Deep Bed Filtration Analysis*, SN Appl Sci., **2**, 1537, 2020. DOI:10.1007/s42452-020-03356-z.

[7] Yu, B. & Li, J., *ERRATUM: Some Fractal Characters of Porous Media*, Fractals, **10**, pp. 365-372, 2002. DOI:10.1142/S0218348X02001300.

[8] Li, C., Shen, Y., Ge, H., Su, S. & Yang, Z., *Analysis of Spontaneous Imbibition in Fractal Tree-like Network System*, Fractals, **24**, pp. 1-12, 2016. DOI:10.1142/S0218348X16500353.

[9] Yu, B. & Cheng, P., *A Fractal Permeability Model for Bi-Dispersed Porous Media*, Int J Heat Mass Transf., **45**, pp. 2983-2993, 2002. DOI:10.1016/S0017-9310(02)00014-5.

[10] Xu, P. & Yu, B., *Developing a New Form of Permeability and Kozeny–Carman Constant for Homogeneous Porous Media by Means of Fractal Geometry*, Adv Water Resour., **31**, pp. 74-81, 2008. DOI: 10.1016/j.advwatres.2007.06.003.

[11] Saafan, M. & Ganat, T., *A New Capillary Pressure Model from Fractal Characterization of Porous Medium: A Case Study from Malaysia*, Solid State Technol., **63**, pp. 936-946, 2020.

[12] Saafan, M. & Ganat, T., *Inferring Capillary Pressure Curve from 2D Rock Images Based on Fractal Theory in Low-Permeability Sandstone: A New Integrated Approach*, Fractals, **29**, 2150149, 2021. DOI:10.1142/ S0218348X21501498.

.

[13] Saafan, M., Ganat, T., Mohyaldinn, M. & Chen, X., *A Fractal Model for Obtaining Spontaneous Imbibition Capillary Pressure Curves Based on 2D Image Analysis of Low-Permeability Sandstone*, J Pet Sci Eng, **208,** 109747, 2022. DOI: 10.1016/j.petrol.2021.109747.

[14] Meng, H., Shi, Q., Liu, T., Liu, F. & Chen, P.*, The Percolation Properties of Electrical Conductivity and Permeability for Fractal Porous Media*, Energies, **12**, 1085, 2019. DOI:10.3390/en12061085.

[15] Wei, W., Cai, J., Hu, X. & Han, Q., *An Electrical Conductivity Model for Fractal Porous Media*, Geophys Res Lett., **42**, pp. 4833-4840, 2015. DOI: 10.1002/2015GL064460.

[16] Li, K., *More General Capillary Pressure and Relative Permeability Models from Fractal Geometry*, J. Contam Hydrol., **111**, pp. 13-24, 2010. DOI: 10.1016/j.jconhyd.2009.10.005.

[17] Cai, J., Hu, X., Standnes, D.C. & You, L., *An Analytical Model for Spontaneous Imbibition in Fractal Porous Media Including Gravity*. Colloids Surfaces A Physicochem Eng., Asp., **414**, pp. 228-233, 2012. DOI: 10.1016/j.colsurfa.2012.08.047.

[18] Gao, H., Yu, B., Duan, Y. & Fang, Q., *Fractal Analysis of Dimensionless Capillary Pressure Function*, Int. J. Heat Mass. Transf., **69**, pp. 26-33, 2014. DOI: 10.1016/j.ijheatmasstransfer.2013.10.006.

[19] Patzek, T.W. & Silin, D.B., *Shape Factor and Hydraulic Conductance in Noncircular Capillaries*, J. Colloid Interface Sci., **236**, pp. 295-304, 2001. DOI: 10.1006/jcis.2000.7413.

[20] Wu, Y., Tahmasebi, P., Lin, C., Zahid, M.A., Dong, C. & Golab, A.N., *A Comprehensive Study on Geometric, Topological and Fractal Characterizations of Pore Systems in Low-Permeability Reservoirs Based On SEM, MICP, NMR, and X-Ray CT Experiments*, Mar Pet Geol., **103**, pp. 12-28, 2019. DOI: 10.1016/j.marpetgeo.2019.02.003.

[21] Piri, M. & Blunt, M.J., *Three-Phase Threshold Capillary Pressures in Noncircular Capillary Tubes with Different Wettabilities Including Contact Angle Hysteresi*s, Phys. Rev. E., **70**, 061603, 2004. DOI: 10.1103/PhysRevE.70.061603.

[22] Khaz'ali, A.R. & Moghadasi, J., *Capillary-Dominated Two-Phase Flow Modeling in Porous Media Using Starfish*, J. Pet. Explor. Prod. Technol., **9**, pp. 1211-1223, 2019. DOI:10.1007/s13202-018-0529-1.

[23] Holland, J.H., *Genetic Algorithms and Adaptation,* in: Selfridge OG, Rissland EL, Arbib MA, editors. Adapt. Control III-Defined Syst., Boston, MA: Springer US, pp. 317-333, 1984. DOI:10.1007/978-1-4684-8941-5_21.

[24] Negnevitsky, M., *Artificial Intelligence: A Guide to Intelligent Systems*, Second Ed Addison-Wesley 2005.